

Optimisation of a Brownian dynamics algorithm for semidilute polymer solutions

Aashish Jain,¹ P. Sunthar,² B. Dünweg,^{3,1} and J. Ravi Prakash^{1,*}

¹*Department of Chemical Engineering, Monash University, Melbourne, VIC 3800, Australia*

²*Department of Chemical Engineering, Indian Institute of Technology Bombay, Powai, Mumbai - 400076, India*

³*Max Planck Institute for Polymer Research, Ackermannweg 10, 55128 Mainz, Germany*

(Dated: March 26, 2018)

Simulating the static and dynamic properties of semidilute polymer solutions with Brownian dynamics (BD) requires the computation of a large system of polymer chains coupled to one another through excluded-volume and hydrodynamic interactions. In the presence of periodic boundary conditions, long-ranged hydrodynamic interactions are frequently summed with the Ewald summation technique. By performing detailed simulations that shed light on the influence of several tuning parameters involved both in the Ewald summation method, and in the efficient treatment of Brownian forces, we develop a BD algorithm in which the computational cost scales as $O(N^{1.8})$, where N is the number of monomers in the simulation box. We show that Beenakker's original implementation of the Ewald sum, which is only valid for systems without bead overlap, can be modified so that θ -solutions can be simulated by switching off excluded-volume interactions. A comparison of the predictions of the radius of gyration, the end-to-end vector, and the self-diffusion coefficient by BD, at a range of concentrations, with the hybrid Lattice Boltzmann/Molecular Dynamics (LB/MD) method shows excellent agreement between the two methods. In contrast to the situation for dilute solutions, the LB/MD method is shown to be significantly more computationally efficient than the current implementation of BD for simulating semidilute solutions. We argue however that further optimisations should be possible.

PACS numbers: 05.10.-a, 05.10.Gg, 47.11.-j, 47.57.Ng, 83.10.Mj, 61.25.he, 83.80.Rs

Keywords: semidilute polymer solutions; hydrodynamic interactions; Ewald summation; Brownian dynamics simulation

I. INTRODUCTION

Understanding the behaviour of polymer solutions in the semidilute regime of concentration is important both from the point of view of applications, and from the point of view of advancing fundamental knowledge in polymer science. Until recently, insight into semidilute polymer solution behaviour was largely obtained through approximate analytical and scaling theories [1–8]. However, significant progress in the development of mesoscopic simulation techniques [9–11], which allow the exploitation of underlying theories without the need for approximations, has made it possible for the first time to obtain detailed predictions of equilibrium and nonequilibrium properties that can be compared with experimental observations. The successful implementation of mesoscopic simulations has been made possible through the use of algorithms that enable an accurate depiction of the semidilute regime. Essentially, this requires the ability to describe long polymers that overlap with each other, while maintaining a low segment density. Further, the segments must be capable of interacting with each other through solvent-mediated hydrodynamic interactions [2, 9, 12–14]. Three different mesoscopic simulation methods, all of which use coarse-grained bead-spring chain models for polymer molecules, have been developed

recently that achieve these objectives. Two of these techniques, namely, the hybrid Lattice Boltzmann/Molecular Dynamics (LB/MD) method [15, 16] and the hybrid Multiparticle Collision Dynamics/Molecular Dynamics (MPCD) method [17–19] treat the solvent explicitly. As a consequence, hydrodynamic interactions between polymer segments arise naturally through the exchange of momentum between the beads on a chain and solvent molecules. In the third approach [10], which is Brownian dynamics (BD) simulations [20], the solvent degrees of freedom are removed completely, but their effect is taken into account through long-range dynamic correlations in the stochastic displacements of the beads. The very nature of semidilute polymer solutions, particularly the need to use periodic boundary conditions to describe homogeneous polymer solutions in unbounded domains, necessitates the simulation of a large number of particles. As a result, the computational efficiency of a simulation technique becomes an important consideration.

To our knowledge, there has been no systematic investigation to compare the performance of the different techniques in terms of their computational efficiency in the semidilute regime. Recently, however, a quantitative comparison of the predictions of the explicit solvent LB/MD method with the predictions of the implicit solvent BD method for the dynamics of a single chain in a solvent, i.e. in the dilute regime, has been carried out with a view to compare their computational efficiencies [21, 22]. It was shown by Pham *et al.* [21] that in order to observe the system for the same time span in physical units, significantly less CPU time is required with BD

* Email: ravi.jagadeeshan@monash.edu
URL: <http://users.monash.edu.au/~rprakash/>

in comparison to LB/MD, for bead-spring chains with $N_b \lesssim 10^6$, where N_b is the number of beads per chain. The situation, however, is expected to be quite different in the semidilute regime. For the LB/MD method, the CPU cost scales linearly with the number of particles, which implies that the CPU cost grows as L^3 since the solvent particles (the calculation of whose dynamics dominates the CPU cost), are distributed on lattice grid points in a simulation box of size L . In order to prevent a chain from wrapping over itself due to spatial restriction and hence altering its static conformation, it is necessary to ensure that $L \geq 2\sqrt{\langle R_e^2 \rangle}$, where $\langle R_e^2 \rangle$ is the mean-square end-to-end distance of the chain. In the dilute case, this leads to the CPU time scaling as $N_b^{3\nu}$ for the LB/MD method, where ν is the Flory exponent. Using a simple scaling argument based on the blob picture of semidilute solutions [3], Pham *et al.* [21] suggest that the CPU effort is even somewhat decreased in semidilute solutions due to the shrinkage of the chains resulting from the screening of excluded-volume interactions [3, 23] — note that this argument is based upon considering the smallest possible system size.

In the case of BD, even though the number of degrees of freedom is significantly reduced by eliminating the solvent, implementation of pairwise hydrodynamic interactions between segments proves to be extremely computationally expensive. For dilute polymer solutions, the computational cost of evaluating intramolecular hydrodynamic interactions arises from the need to carry out a decomposition of the diffusion tensor that appears in the stochastic equation of motion. A straightforward Cholesky decomposition leads to an algorithm that scales like $O(N_b^3)$. Many current implementations of single chain BD simulations, however, mitigate this large CPU cost by using Fixman’s polynomial approximation to this decomposition, which leads to $O(N_b^{2.25})$ scaling [24–27]. In the case of semidilute polymer solutions, both intramolecular and intermolecular hydrodynamic interactions must be taken into account. The use of periodic boundary conditions to imitate bulk systems necessitates the evaluation of hydrodynamic interactions not only between one particular chosen segment and all other segments within the primary simulation box, but also with all the other segments in all the periodic images of the box. Because of the long-range nature of hydrodynamic interactions, which decay only reciprocally with distance, this sum converges very slowly and only conditionally [28, 29]. Inspired by its earlier success in summing electrostatic interaction (which are also long-ranged in nature), the problem of slow convergence has been resolved through the use of the Ewald summation technique [30–34] — both in the context of BD simulations of colloidal suspensions where hydrodynamic interactions between particles with a finite radius must be taken into account [35–39], and in the context of BD simulations of semidilute polymer solutions where the polymer segments are assumed to be point particles [10].

Rapid convergence is achieved in the Ewald method

by splitting the original expression into two sums, one of them in real space and the other in reciprocal space, both of which converge exponentially. A straightforward implementation of the Ewald sum, however, is computationally demanding, scaling like $O(N^2)$, where $N = N_c \times N_b$, is the total number of beads in the primary simulation box with N_c polymer chains. Interestingly, by a suitable choice of a parameter α in the Ewald sum that tunes the relative weights of the real space and reciprocal space contributions (consequently splitting the load of calculating the total sum between the real space and reciprocal space sums), it is possible to make the computational cost of calculating either the real space or the reciprocal space sum scale like $O(N^2)$, while the remaining sum scales as $O(N)$. In their recent simulation of semidilute polymer solutions, Stoltz *et al.* [10] have implemented a BD algorithm that leads to the real space sum scaling like $O(N^2)$. In the case of colloidal suspensions, accelerated BD algorithms have been developed by Brady and co-workers with the Ewald sum scaling like $O(N \log N)$ [38, 39]. The essential idea is to retain an $O(N)$ scaling for the real space sum, while reducing the complexity of the reciprocal part of the Ewald sum to $O(N \log N)$ with the help of Fast Fourier Transformation. For confined systems which are non-periodic, and in which methods based on Fourier transforms are not applicable, the Wisconsin group have recently successfully introduced a BD simulation technique they term the “general geometry Ewald-like method”, which achieves $O(N \log N)$ scaling [40]. Analogous to the Ewald method, the technique is based on splitting the solution to the Stokes equation into singular short-ranged parts and smooth long-ranged parts. Thus, even though a detailed quantitative comparison of all the currently available mesoscopic simulation techniques is yet to be carried out, they all appear to scale, in their most efficient versions, roughly linearly with system size.

In the context of electrostatic interactions, two different classes of schemes have been proposed for the optimisation of the Ewald sum [31, 34, 41, 42]. One of these classes (on which the accelerated BD schemes are modelled), achieves $O(N \log N)$ scaling by assigning particles to a mesh and then using Fast Fourier Transform techniques to evaluate the reciprocal-space part of the Ewald sum on this mesh [32, 34]. The other class [41, 42] achieves $O(N^{1.5})$ scaling by balancing the computational cost of evaluating the real space and reciprocal space sums, i.e. by an optimal choice of the aforementioned parameter α . To our knowledge, the latter approach has so far not been trialled for summing hydrodynamic interactions.

In the context of hydrodynamic interactions, it is also worth noting that the BD simulation of semidilute polymer solutions carried out by Stoltz *et al.* [10] differs from BD simulations of colloidal suspensions [36, 39] in the procedure adopted for the calculation of *far-field* hydrodynamic interactions, even though both are based on the Ewald summation technique. While the latter are based

on Hasimoto's solution of the Stokes equation for flow past a periodic array of point forces [28], i.e. on the Ewald sum of the Oseen-Burgers tensor, the former is based on Beenakker's solution [29], which is the Ewald sum of the Rotne-Prager-Yamakawa (RPY) tensor. The RPY tensor [20, 43, 44] is a generalisation of the Oseen-Burgers tensor in two aspects: Firstly, it approximately takes into account the finite particle radius by representing the far-field hydrodynamic flow field up to quadrupolar order of its multipole expansion [45] (Oseen-Burgers is just a monopole field), and, secondly, it regularises the singularity that occurs for small inter-bead distances. Such a regularisation is necessary for BD simulations that allow for configurations with overlapping beads, since otherwise the diffusion tensor would not always be positive-definite, implying a violation of the second law of thermodynamics. The problem can be avoided by introducing sufficiently strong excluded-volume interactions, which suppress the occurrence of such configurations; this was the approach taken by Stoltz *et al.* [10]. By this procedure, they also avoided the problem that Beenakker's formulae [29] are applicable only to the far-field branch of the RPY tensor and not to the regularised near-field branch. However, one can anticipate that bead overlap will occur in simulations of semidilute θ -solutions, since θ -solutions are commonly simulated by switching off excluded-volume interactions [27, 46]. We therefore develop in the present paper a method that is able to deal with overlaps, by implementing the Ewald sum of *both branches* of the RPY tensor. It should be noted that the near-field RPY formula is not the only possible regularisation that has been discussed in the literature; an alternative was suggested in Ref. 47. While the details of the regularisation are unlikely to significantly affect the dynamic properties of semidilute polymer solutions, we have focused on the RPY formula, since, according to our knowledge, it is the only known regularisation that provenly provides positive-definiteness for all chain lengths and configurations [20]. For a physical motivation of the RPY regularisation, see Ref. [43]. In the context of BD simulations of colloidal suspensions, the problem of positive-definiteness does not arise due to excluded-volume interactions, while *near-field* hydrodynamic interactions are taken into account through short-range lubrication forces [36].

In this paper, four aspects of the implementation and optimisation of BD simulations for semidilute polymer solutions are considered: (i) The development of an algorithm that scales like $O(N^{1.5})$ for calculating pair-wise hydrodynamic interactions in periodic systems; (ii) The derivation of a modified version of Beenakker's periodic RPY tensor that is applicable to simulations of solutions under θ conditions; (iii) The optimal implementation of Fixman's polynomial approximation to the decomposition of the diffusion tensor, within the context of the current BD simulation algorithm and (iv) Optimisation of the overall algorithm for a single Euler time step. Finally, the resulting optimised BD algorithm has been used to

calculate a variety of equilibrium properties of semidilute polymer solutions, across a range of concentrations, and compared quantitatively with the results of the LB/MD algorithm, along with a comparison of the CPU time scaling for both these approaches.

The plan of the paper is as follows. In Sec. II, the governing equations, along with the implementation of the Ewald sum and its modification to handle overlapping beads, are discussed. Sections III, IV, and V consider the optimisation of (i) the Ewald sum for hydrodynamic interactions, (ii) the Chebychev polynomial approximation for the decomposition of the diffusion tensor, and (iii) the execution of a single Euler time step, respectively. The optimised BD algorithm is validated by a variety of different means, under both θ and good solvent conditions, in Sec. VI, and in Sec. VII, its computational cost is compared with that of the LB/MD method at a concentration that lies in the semidilute regime. Finally, the principal conclusions are summarised in Sec. VIII.

II. MODEL AND SIMULATION METHOD

A. Governing equation

A linear bead-spring chain model is used to represent polymers at the mesoscopic level, with each polymer chain coarse-grained into a sequence of N_b beads, which act as centres of hydrodynamic resistance, connected by $N_b - 1$ massless springs that represent the entropic force between adjacent beads. A semidilute polymer solution is modelled as an ensemble of such bead-spring chains, immersed in an incompressible Newtonian solvent. A total of N_c chains are initially enclosed in a cubic and periodic cell of edge length L , giving a total of $N = N_b \times N_c$ beads per cell at a bulk monomer concentration of $c = N/V$, where $V = L^3$ is the volume of the simulation cell. Using the length scale $l_H = \sqrt{k_B T/H}$ and time scale $\lambda_H = \zeta/4H$, where k_B is the Boltzmann's constant, T is the temperature, H is the spring constant and ζ is the hydrodynamic friction coefficient associated with a bead, the Euler integration algorithm for the non-dimensional Ito stochastic differential equation governing the position vector $\mathbf{r}_\nu(t)$ of bead ν at time t , is [10]

$$\begin{aligned} \mathbf{r}_\nu(t + \Delta t) = & \mathbf{r}_\nu(t) + [\boldsymbol{\kappa} \cdot \mathbf{r}_\nu(t)] + \frac{\Delta t}{4} \sum_{\mu=1}^N [\mathbf{D}_{\nu\mu}(t) \cdot \mathbf{F}_\mu(t)] \\ & + \frac{1}{\sqrt{2}} \sum_{\mu=1}^N [\mathbf{B}_{\nu\mu}(t) \cdot \Delta \mathbf{W}_\mu(t)] \end{aligned} \quad (1)$$

Here, the 3×3 tensor $\boldsymbol{\kappa}$ is equal to $(\nabla \mathbf{v})^T$, with \mathbf{v} being the unperturbed solvent velocity. The dimensionless diffusion tensor $\mathbf{D}_{\nu\mu}$ is a 3×3 matrix for a fixed pair of beads μ and ν . It is related to the hydrodynamic interaction tensor, as discussed further subsequently. \mathbf{F}_μ incorporates all the non-hydrodynamic forces on bead μ

due to all the other beads. The components of the Gaussian noise $\Delta \mathbf{W}_\mu$ are obtained from a real-valued Gaussian distribution with zero mean and variance Δt . The quantity $\mathbf{B}_{\nu\mu}$ is a non-dimensional tensor whose presence leads to multiplicative noise [20]. Its evaluation requires the decomposition of the diffusion tensor. Defining the matrices \mathcal{D} and \mathcal{B} as block matrices consisting of $N \times N$ blocks each having dimensions of 3×3 , with the (ν, μ) -th block of \mathcal{D} containing the components of the diffusion tensor $\mathbf{D}_{\nu\mu}$, and the corresponding block of \mathcal{B} being equal to $\mathbf{B}_{\nu\mu}$, the decomposition rule for obtaining \mathcal{B} can be expressed as

$$\mathcal{B} \cdot \mathcal{B}^T = \mathcal{D} \quad (2)$$

The non-hydrodynamic forces in the model are comprised of the spring forces $\mathbf{F}_\mu^{\text{spr}}$ and excluded-volume interaction forces $\mathbf{F}_\mu^{\text{exv}}$, i.e., $\mathbf{F}_\mu = \mathbf{F}_\mu^{\text{spr}} + \mathbf{F}_\mu^{\text{exv}}$. A linear Hookean spring potential is used here for modelling the spring forces when considering the optimisation of the Ewald sum, while a finitely extensible nonlinear elastic (FENE) potential has been used while comparing results with the Lattice Boltzmann method. The entropic spring force on bead μ due to adjacent beads can be expressed as $\mathbf{F}_\mu^{\text{spr}} = \mathbf{F}^c(\mathbf{Q}_\mu) - \mathbf{F}^c(\mathbf{Q}_{\mu-1})$ where $\mathbf{F}^c(\mathbf{Q}_{\mu-1})$ is the force between the beads $\mu-1$ and μ , acting in the direction of the connector vector between the two beads $\mathbf{Q}_{\mu-1} = \mathbf{r}_\mu - \mathbf{r}_{\mu-1}$. The dimensionless Hookean spring force is given by $\mathbf{F}^c(\mathbf{Q}_\mu) = \mathbf{Q}_\mu$, while for FENE springs, $\mathbf{F}^c(\mathbf{Q}_\mu) = \frac{\mathbf{Q}_\mu}{1 - |\mathbf{Q}_\mu|^2/b}$, where $b = Hq_0^2/k_B T$ is the dimensionless finite extensibility parameter, and q_0 is the dimensional maximum stretch of a spring.

The non-dimensional diffusion tensor $\mathbf{D}_{\nu\mu}$ in Eq. (1) is related to the non-dimensional hydrodynamic interaction tensor \mathcal{O} through

$$\mathbf{D}_{\mu\nu} = \delta_{\mu\nu} \boldsymbol{\delta} + (1 - \delta_{\mu\nu}) \mathcal{O}(\mathbf{r}_\nu - \mathbf{r}_\mu) \quad (3)$$

where $\boldsymbol{\delta}$ and $\delta_{\mu\nu}$ represent a unit tensor and a Kronecker delta, respectively, while \mathcal{O} represents the effect of the motion of a bead μ on another bead ν through the disturbances carried by the surrounding fluid. The hydrodynamic interaction tensor \mathcal{O} is assumed to be given by the Rotne-Prager-Yamakawa (RPY) regularisation of the Oseen function

$$\mathcal{O}(\mathbf{r}) = \Omega_1 \boldsymbol{\delta} + \Omega_2 \frac{\mathbf{r}\mathbf{r}}{r^2} \quad (4)$$

where for $r \geq 2a$, the *branch* \mathcal{A} of the RPY functions Ω_1 and Ω_2 is given by, respectively,

$$\Omega_1 = \frac{3a}{4r} \left(1 + \frac{2a^2}{3r^2} \right) \quad \text{and} \quad \Omega_2 = \frac{3a}{4r} \left(1 - \frac{2a^2}{r^2} \right) \quad (5)$$

while for $0 < r \leq 2a$, the *branch* \mathcal{B} of the RPY functions Ω_1 and Ω_2 is given by, respectively,

$$\Omega_1 = 1 - \frac{9}{32} \frac{r}{a} \quad \text{and} \quad \Omega_2 = \frac{3}{32} \frac{r}{a} \quad (6)$$

We introduce the notation of the two branches \mathcal{A} and \mathcal{B} for facilitating subsequent discussion. The quantity a has been introduced here as the non-dimensional radius of the bead as an additional independent parameter. It is related to the conventionally defined [48, 49] hydrodynamic interaction parameter h^* by $a = \sqrt{\pi} h^*$. As is well known [29], the sum $\sum_\mu \mathbf{D}_{\nu\mu} \cdot \mathbf{F}_\mu$ in Eq. (1) converges slowly since $\mathbf{D}_{\mu\nu}$ is long-ranged in nature, scaling as $1/r$. The problem of slow convergence can be resolved through the use of the Ewald sum, as discussed in greater detail below. It is worth noting here that it is sufficient to evaluate $\sum_\mu \mathbf{D}_{\nu\mu} \cdot \mathbf{F}_\mu$ in order to determine the time evolution of $\mathbf{r}_\nu(t)$. It is not necessary to know $\mathbf{D}_{\nu\mu}$ explicitly. Further, as will be seen later, the evaluation of $\sum_\mu \mathbf{B}_{\nu\mu} \cdot \Delta \mathbf{W}_\mu$ using a Chebyshev polynomial approximation for $\mathbf{B}_{\nu\mu}$, also requires a repeated evaluation of the Ewald sum.

B. Evaluation of $\sum_\mu \mathbf{D}_{\nu\mu} \cdot \mathbf{F}_\mu$ as an Ewald sum

Beenakker's [29] representation of the sum $\sum_\mu \mathbf{D}_{\nu\mu} \cdot \mathbf{F}_\mu$ as an Ewald sum for infinite periodic systems, using the RPY tensor to represent hydrodynamic interactions, has the form

$$\begin{aligned} \sum_{\mu=1}^N \mathbf{D}_{\nu\mu} \cdot \mathbf{F}_\mu &= \left(1 - \frac{6a\alpha}{\sqrt{\pi}} + \frac{40a^3 \alpha^3}{3\sqrt{\pi}} \right) \mathbf{F}_\nu \\ &+ \sum_{\mathbf{n}}' \sum_{\mu=1}^N \mathbf{M}^{(1)}(\mathbf{r}_{\nu\mu,\mathbf{n}}) \cdot \mathbf{F}_\mu + \sum_{\mathbf{k} \neq \mathbf{0}} \mathbf{M}^{(2)}(\mathbf{k}) \cdot \\ &\left\{ \cos(\mathbf{k} \cdot \mathbf{r}_\nu) \sum_{\mu=1}^N \cos(\mathbf{k} \cdot \mathbf{r}_\mu) \mathbf{F}_\mu \right. \\ &\left. - \sin(\mathbf{k} \cdot \mathbf{r}_\nu) \sum_{\mu=1}^N \sin(\mathbf{k} \cdot \mathbf{r}_\mu) \mathbf{F}_\mu \right\} \quad (7) \end{aligned}$$

where the first and the second sums on the right hand side, both of which converge rapidly, are carried out in real and reciprocal space, respectively. The first term on the RHS is the correction due to self-interactions and does not involve any summation. The parameter α determines the manner in which the computational burden is split between the two sums. The vector $\mathbf{r}_{\nu\mu,\mathbf{n}}$ is defined by $\mathbf{r}_{\nu\mu,\mathbf{n}} = \mathbf{r}_\nu - \mathbf{r}_\mu + \mathbf{n}L$, where $\mathbf{n} = (n_x, n_y, n_z)$ is the lattice vector with n_x, n_y, n_z being integer numbers (see Fig. 1). The first summation on the RHS of Eq. (7) is carried out in the original simulation box and over all the neighbouring periodic images. The prime on the summation indicates that the lattice vector $\mathbf{n} = \mathbf{0}$ is omitted for $\nu = \mu$. $\mathbf{M}^{(1)}(\mathbf{r})$ is a 3×3 matrix (in real space), which depends on a and α , and $\mathbf{M}^{(2)}(\mathbf{k})$ is also a 3×3 matrix (in reciprocal space), which depends on a, α and the volume of the simulation box V . The expressions for $\mathbf{M}^{(1)}(\mathbf{r})$ and

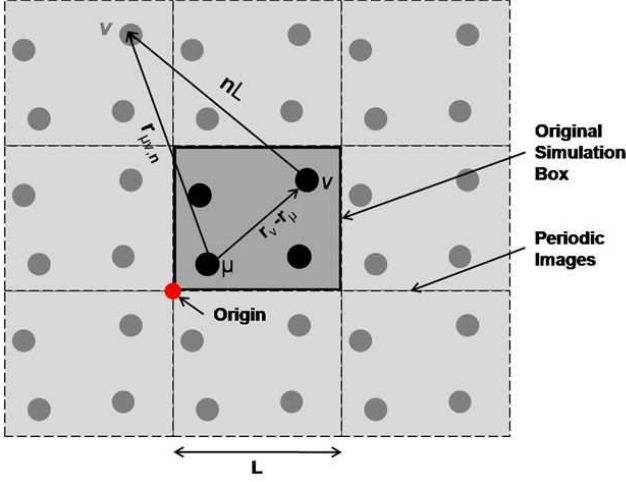


FIG. 1. (Color online) Periodic boundary conditions in 2-D: demonstration of the distance vector between two beads

$\mathbf{M}^{(2)}(\mathbf{k})$ are

$$\begin{aligned} \mathbf{M}^{(1)}(\mathbf{r}) = & \left[\operatorname{erfc}(\alpha r) \left(\frac{3a}{4r} + \frac{a^3}{2r^3} \right) \right. \\ & + \frac{\exp(-\alpha^2 r^2)}{\sqrt{\pi}} \left(3a\alpha^3 r^2 - \frac{9a\alpha}{2} + 4a^3\alpha^7 r^4 \right. \\ & \left. \left. - 20a^3\alpha^5 r^2 + 14a^3\alpha^3 + \frac{a^3\alpha}{r^2} \right) \right] \boldsymbol{\delta} \\ & + \left[\operatorname{erfc}(\alpha r) \left(\frac{3a}{4r} - \frac{3a^3}{2r^3} \right) \right. \\ & + \frac{\exp(-\alpha^2 r^2)}{\sqrt{\pi}} \left(\frac{3a\alpha}{2} - 3a\alpha^3 r^2 - 4a^3\alpha^7 r^4 \right. \\ & \left. \left. + 16a^3\alpha^5 r^2 - 2a^3\alpha^3 - \frac{3a^3\alpha}{r^2} \right) \right] \hat{\mathbf{r}}\hat{\mathbf{r}} \quad (8) \end{aligned}$$

with erfc denoting the complementary error function, and

$$\begin{aligned} \mathbf{M}^{(2)}(\mathbf{k}) = & \left(a - \frac{a^3 k^2}{3} \right) \left(1 + \frac{k^2}{4\alpha^2} + \frac{k^4}{8\alpha^4} \right) \\ & \left(\frac{6\pi}{k^2 V} \right) \exp\left(\frac{-k^2}{4\alpha^2}\right) \left(\boldsymbol{\delta} - \hat{\mathbf{k}}\hat{\mathbf{k}} \right) \quad (9) \end{aligned}$$

The second summation in Eq. (7) (denoted here as the reciprocal space sum) is carried out over lattice vectors $\mathbf{k} = 2\pi\mathbf{n}/L$. In Eq. (8), r and $\hat{\mathbf{r}}$ are the magnitude and unit vector, respectively, in the direction of \mathbf{r} . In Eq. (9), k and $\hat{\mathbf{k}}$ are the magnitude and unit vector, respectively, corresponding to \mathbf{k} .

C. Modification of the Ewald sum to account for overlapping beads

As pointed out earlier, the derivation of the Ewald sum by Beenakker [29] is valid *only* for the branch \mathcal{A} of the

RPY functions Ω_1 and Ω_2 (Eq. (5)), which forbids its use for the case of overlapping beads ($r < 2a$). The original expression consequently cannot be used for the simulation of θ solvents by neglecting excluded-volume interactions, as in this case beads on the same or on different chains are highly prone to overlap with each other. The Ewald sum has been modified here to account for such situations.

Starting from a given bead ν , we consider all those beads that have distances less than $2a$ from it, including bead ν itself. By a proper re-labeling, we can assume that these are the beads $\mu = 1, \dots, N^*$. The number of non-overlapping particles is thus $N - N^*$. As the correction needs to be carried out only in the real space sum, the first summation on the RHS of Eq. (7) $\left(\sum_{\mathbf{n}} \sum_{\mu=1}^N \mathbf{M}^{(1)}(\mathbf{r}_{\nu\mu,\mathbf{n}}) \cdot \mathbf{F}_{\mu} \right)$ is replaced by

$$\begin{aligned} & \sum_{\substack{\mu=1 \\ \mu \neq \nu}}^{N^*} \mathbf{M}_{\mathbf{B}}^{(1)}(\mathbf{r}_{\nu\mu,\mathbf{n}=0}) \cdot \mathbf{F}_{\mu} + \sum_{\mathbf{n} \neq 0} \sum_{\mu=1}^{N^*} \mathbf{M}^{(1)}(\mathbf{r}_{\nu\mu,\mathbf{n}}) \cdot \mathbf{F}_{\mu} \\ & + \sum_{\mathbf{n}} \sum_{\mu=N^*+1}^N \mathbf{M}^{(1)}(\mathbf{r}_{\nu\mu,\mathbf{n}}) \cdot \mathbf{F}_{\mu} \quad (10) \end{aligned}$$

where the first summation of Eq. (10) is carried out only over overlapping particles in the original simulation box ($\mathbf{n} = \mathbf{0}$). Similar to Beenakker's [29] derivation of the $\mathbf{M}^{(1)}$ matrix, the matrix $\mathbf{M}_{\mathbf{B}}^{(1)}$ is derived here based on the branch \mathcal{B} of the RPY tensor given by Eq. (6). The second summation is carried out over the periodic images of the overlapping particles (whose distances are more than $2a$), and the third summation is similar to that given in Eq. (7) but here it is carried out only over the non-overlapping particles. Note that the second sum is not carried out in the original box. In order to make this sum extend over the original box and periodic images, a term is added and subtracted as follows

$$\begin{aligned} & \sum_{\substack{\mu=1 \\ \mu \neq \nu}}^{N^*} \mathbf{M}_{\mathbf{B}}^{(1)}(\mathbf{r}_{\nu\mu,\mathbf{n}=0}) \cdot \mathbf{F}_{\mu} + \sum_{\mathbf{n} \neq 0} \sum_{\mu=1}^{N^*} \mathbf{M}^{(1)}(\mathbf{r}_{\nu\mu,\mathbf{n}}) \cdot \mathbf{F}_{\mu} \\ & + \sum_{\substack{\mu=1 \\ \mu \neq \nu}}^{N^*} \mathbf{M}^{(1)}(\mathbf{r}_{\nu\mu,\mathbf{n}=0}) \cdot \mathbf{F}_{\mu} - \sum_{\substack{\mu=1 \\ \mu \neq \nu}}^{N^*} \mathbf{M}^{(1)}(\mathbf{r}_{\nu\mu,\mathbf{n}=0}) \cdot \mathbf{F}_{\mu} \\ & + \sum_{\mathbf{n}} \sum_{\mu=N^*+1}^N \mathbf{M}^{(1)}(\mathbf{r}_{\nu\mu,\mathbf{n}}) \cdot \mathbf{F}_{\mu} \quad (11) \end{aligned}$$

The second, third and fifth summations of the above equation together represent the original real space sum in Eq. (7). Eq. (11) can consequently be rearranged as

$$\begin{aligned} & \left(\sum_{\mathbf{n}} \sum_{\mu=1}^N \mathbf{M}^{(1)}(\mathbf{r}_{\nu\mu,\mathbf{n}}) \cdot \mathbf{F}_{\mu} \right) \\ & + \sum_{\substack{\mu=1 \\ \mu \neq \nu}}^{N^*} \left[\mathbf{M}_{\mathbf{B}}^{(1)}(\mathbf{r}_{\nu\mu,\mathbf{n}=0}) - \mathbf{M}^{(1)}(\mathbf{r}_{\nu\mu,\mathbf{n}=0}) \right] \cdot \mathbf{F}_{\mu} \quad (12) \end{aligned}$$

where the second summation is carried over all overlapping particles in the original box. Denoting the second term in Eq. (12) by \mathbf{M}^* , it is straightforward to show that

$$\begin{aligned} \mathbf{M}^*(\mathbf{x}) = & \left[1 - \frac{1}{2x^3} \left(\frac{3x^2}{4} + 1 \right)^2 \right] \boldsymbol{\delta} \\ & + \left[\frac{1}{2x^3} \left(\frac{3x^2}{4} - 1 \right)^2 \right] \hat{\mathbf{x}} \hat{\mathbf{x}} \end{aligned} \quad (13)$$

where $\mathbf{x} = \mathbf{r}_{(\nu\mu, \mathbf{n}=0)}/a$ and $\hat{\mathbf{x}}$ is the unit vector in the direction of $\mathbf{r}_{(\nu\mu, \mathbf{n}=0)}$. The modified form of the Ewald sum that is valid for arbitrary inter-particle distance is consequently

$$\begin{aligned} & \sum_{\mu=1}^N \mathbf{D}_{\nu\mu} \cdot \mathbf{F}_{\mu} = \left(1 - \frac{6a\alpha}{\sqrt{\pi}} + \frac{40a^3\alpha^3}{3\sqrt{\pi}} \right) \mathbf{F}_{\nu} \\ & + \sum_{\mathbf{n}}' \sum_{\mu=1}^N \mathbf{M}^{(1)}(\mathbf{r}_{\nu\mu, \mathbf{n}}) \cdot \mathbf{F}_{\mu} + \sum_{\mathbf{k} \neq \mathbf{0}} \mathbf{M}^{(2)}(\mathbf{k}) \cdot \\ & \left\{ \cos(\mathbf{k} \cdot \mathbf{r}_{\nu}) \sum_{\mu=1}^N \cos(\mathbf{k} \cdot \mathbf{r}_{\mu}) \mathbf{F}_{\mu} \right. \\ & \left. - \sin(\mathbf{k} \cdot \mathbf{r}_{\nu}) \sum_{\mu=1}^N \sin(\mathbf{k} \cdot \mathbf{r}_{\mu}) \mathbf{F}_{\mu} \right\} \\ & + \sum_{\substack{\mu=1 \\ \mu \neq \nu}}^{N^*} \mathbf{M}^*(\mathbf{r}_{\nu\mu, \mathbf{n}=0}) \cdot \mathbf{F}_{\mu} \end{aligned} \quad (14)$$

D. Implementation of the Ewald sum

As discussed earlier, the real space sum is carried out over all the periodic images while the reciprocal space sum is performed only in the original simulation box. There are three parameters which control the accuracy of both the real and reciprocal space sums: n_{max} , an integer which defines the range of the real space sum (governed by the number of periodic images, see Fig. 1), k_{max} , an integer that defines the summation range in reciprocal space and the Ewald parameter α . These three parameters are related to each other from the point of view of accuracy and speed. A large value of α makes the real space sum converge faster (since a smaller value of n_{max} is required). However, this leads to the reciprocal space sum requiring a larger number of wavevectors k_{max} . On the other hand, a small value of α implies an expensive real space sum but a cheaper reciprocal space sum. The optimal choice of these parameters has been discussed previously by Fincham [42] in the context of electrostatic interactions. Here, a similar study is performed for hydrodynamics interactions.

1. Choice of Ewald parameters

At fixed monomer bulk concentration c , the box size increases as $N^{1/3}$. As can be seen from Eqs. (7) and (8), the convergence of the real space sum depends on the complementary error function $\text{erfc}(\alpha r)$, where r is the distance between a pair of beads. In practice, the sum is evaluated only for $r \leq r_c$, where r_c denotes a *cutoff* radius. The value of α is chosen such that $\text{erfc}(\alpha r_c)$ is small. At large values of the argument, $\text{erfc}(\alpha r_c)$ behaves as $\exp(-\alpha^2 r_c^2)$. If we specify M such that $\exp(-M^2)$ is very small, then

$$\alpha^2 r_c^2 = M^2 \quad \text{or} \quad \alpha = M/r_c \quad (15)$$

Similarly the rate of convergence of the reciprocal space sum is controlled by the factor $\exp(-k^2/4\alpha^2)$. If it is required [42] that the accuracy of the real space sum is roughly equal to that of the reciprocal space sum at the reciprocal space cutoff, K , then using Eq. (15) we find

$$M^2 = K^2/(4\alpha^2) \quad \text{or} \quad K = 2\alpha M = 2M^2/r_c \quad (16)$$

These relations allow us to specify α and K for given values of M and r_c , while the latter parameters control the accuracy and speed of the algorithm, as discussed subsequently.

2. The real space and reciprocal space sums

Locating all pairs of beads which are separated by less than the cutoff distance r_c is the first step in evaluating the real space sum. A naive all-pairs neighbour search results in $O(N^2)$ performance and therefore the link-cell method, which is a cell-based neighbour search method, is used to improve the performance [50–52]. The calculation of the infinite real space sum is thus reduced to the calculation of the sum locally over only a small number of neighbouring beads. Here, the neighbour search is implemented with cells of side $r_c/5$.

The reciprocal space sum is more straightforward to implement. The major effort is expended in the evaluation of terms of the form $\exp(i\mathbf{k} \cdot \mathbf{r}_{\mu})$. The method adopted here precomputes the components of these factors by recursion and stores them [42]. This avoids calling the complex exponential function repeatedly. However, it involves a substantial amount of computer memory.

III. OPTIMISATION OF THE EVALUATION OF $\sum_{\mu} \mathbf{D}_{\nu\mu} \cdot \mathbf{F}_{\mu}$

The Ewald parameter α , which splits the computational burden between the real space sum and the reciprocal space sum, is related to the real space cutoff r_c by Eq. (15). The aim of optimisation is to minimise the total execution time (which is the sum of the real space execution time, T_R and the reciprocal space execution

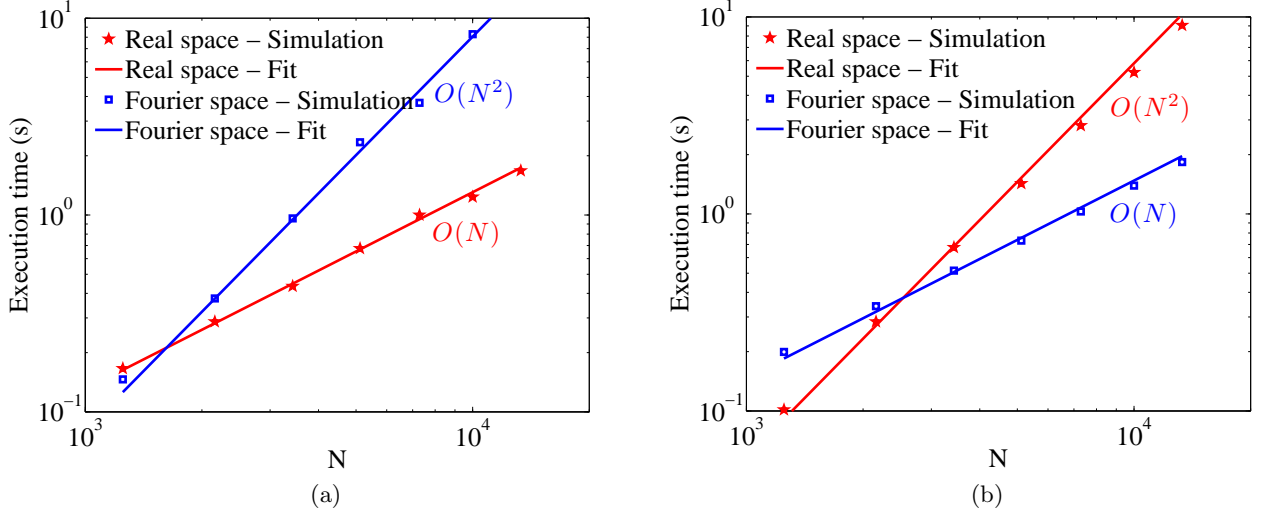


FIG. 2. (Color online) Execution time scaling for the real space and the Fourier space sums for: (a) Constant r_c (b) Constant L/r_c

time, T_F), with respect to the real space cutoff r_c . Following Fincham [42], the execution time T_R is calculated as follows. A sphere of cutoff radius r_c contains on average $N_{r_c} = \frac{4\pi}{3} r_c^3 c$ beads. Each bead interacts with the N_{r_c} beads that surround it. Since for symmetry reasons, each pair interaction needs to be considered only once, the execution time is

$$T_R = \frac{1}{2} A_R N \frac{4\pi}{3} r_c^3 c t_r \quad (17)$$

where A_R is a constant that depends on the code architecture and t_r is the execution time to evaluate one interaction, which is found to be $0.15 \mu s$ when the BD code is run on a 156 SGI Altix XE 320 cluster. Eq. (17) is fit to data obtained by running simulations for a range of parameters on a 156 SGI Altix XE 320 cluster, and the fitted parameter A_R is then found to be 5.

The execution time T_F is evaluated as follows. Within the cutoff K , the volume of the reciprocal space is $\frac{4\pi}{3} K^3 = \frac{4\pi}{3} \frac{8M^6}{r_c^3}$ (the latter follows from Eq. (16)). The reciprocal space points are defined by $k = \frac{2\pi}{L}(l, m, n)$ where l, m, n are integers and L is the simulation box size. The volume of reciprocal space per point is, thus, $(2\pi/L)^3$, and $\frac{4\pi}{3} \frac{8M^6}{r_c^3} \frac{L^3}{8\pi^3}$ is the number of points in the cutoff sphere. Using $L^3 = N/c$ to highlight the N dependence at fixed concentration c , the number of reciprocal space points in the cutoff sphere becomes $\frac{4\pi}{3} \frac{M^6}{\pi^3} \frac{N}{cr_c^3}$. It is worth pointing out that for fixed cutoff radius, the number of k -space points increases as N , because the concentration of points in reciprocal space increases with system size. Further, inversion symmetry of reciprocal space halves the number of reciprocal space points men-

tioned above. A sum over the N beads must be performed for each k -space point, so the execution time is

$$T_F = A_F \frac{1}{2} \frac{4\pi}{3} \frac{M^6}{\pi^3} \frac{N^2}{cr_c^3} t_f \quad (18)$$

where A_F is a code architecture constant and t_f is the execution time to evaluate one term in the sum, which is found to be $0.33 \mu s$. As in the real space instance, Eq. (18) is fitted to simulation data to obtain $A_F = 0.19$. The total execution time is consequently

$$\begin{aligned} T &= T_R + T_F \\ &= \frac{1}{2} \frac{4\pi}{3} \left[A_R N r_c^3 c t_r + A_F \frac{M^6}{\pi^3} \frac{N^2}{cr_c^3} t_f \right] \quad (19) \end{aligned}$$

Equation (19) shows that, for fixed M and r_c , T_R varies as N , but T_F varies as N^2 , because of the increasing concentration of points in reciprocal space. This behaviour is demonstrated for $c = 4.44 c^*$ and $r_c = 10$ in Fig. 2 (a) for the simulation data (symbols), which agrees with the expressions given in Eqs. (17) and (18) (solid lines). Here c^* is the overlap concentration defined by $N_b / \left[\frac{4\pi}{3} (R_g^0)^3 \right]$, where R_g^0 is the radius of gyration of a polymer chain in the dilute limit. To increase the value of N , we fix the value of beads per chain at $N_b = 10$ and increase the number of chains N_c . Conversely, if r_c is increased as the system size increases in such a way that r_c/L is constant (as in the approach adopted by Stoltz *et al.* [10]), then since $c = N/L^3$, T_R varies as N^2 but T_F varies as N . Figure 2 (b) displays this behaviour for $N_b = 10$, $c = 4.44 c^*$, $M = 3.3$ and $L/r_c = 3$. Once again the simulation data is seen to match the expressions given in Eqs. (17) and (18). This suggests that by appropriate choice of parameters it may be possible to achieve better than N^2 behaviour in the total time T . For a given accuracy, the only free parameter is r_c , since this determines

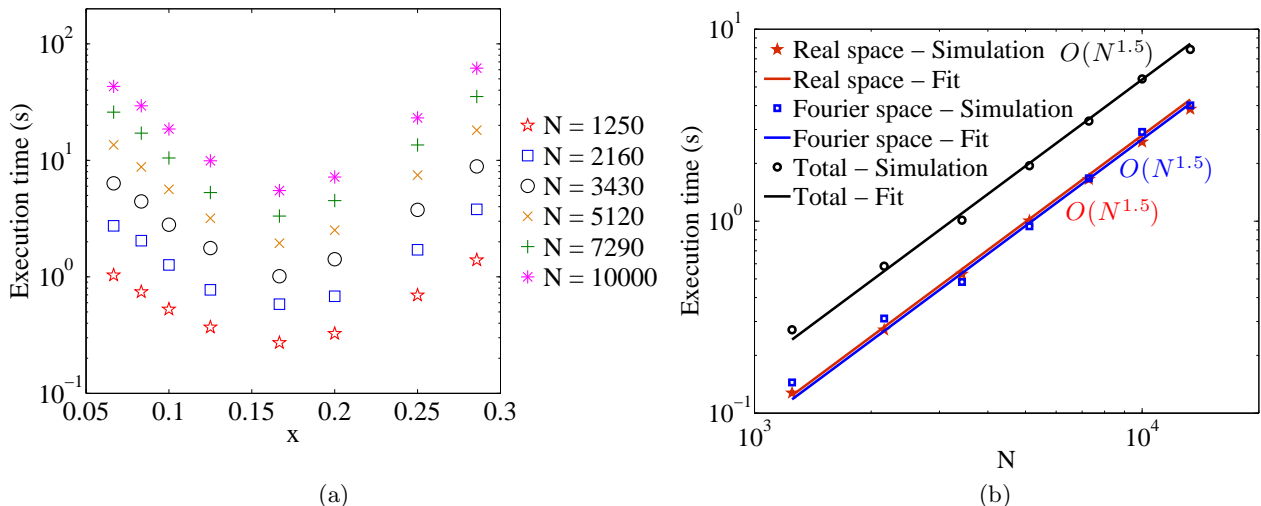


FIG. 3. (Color online) (a) Total execution time vs. exponent x for various N (b) Power law scaling for T_R , T_F and T_{opt} at $(r_c^E)_{\text{opt}}$

α and hence K by Eqs. (15) and (16). To find the value of r_c which minimises the total execution time, we set $dT/dr_c = 0$. This leads to

$$(r_c^E)_{\text{opt}} = \frac{M}{\sqrt{\pi}} \left(\frac{A_F t_f}{A_R t_r} \right)^{1/6} \frac{N^{1/6}}{c^{1/3}} \quad (20)$$

Thus the optimal choice of the cutoff radius $(r_c^E)_{\text{opt}}$ increases slowly (1/6th power) with N . The validity of Eq. (20) has been verified by carrying out simulations. Assuming that the quantity $N^{1/6}$ in Eq. (20) is replaced by N^x , various values of the exponent x are selected in place of the exponent 1/6, and the total execution time for a given value of N is estimated. Fig. 3 (a) shows the total execution time as a function of the exponent x and it is clear that the minimum execution time is achieved when $x = 1/6$ as given by Eq. (20), for all N .

Substituting $(r_c^E)_{\text{opt}}$ in Eq. (19) we find for the optimal time

$$T_{\text{opt}} = 2T_R = 2T_F = \frac{4\pi}{3} N^{1.5} \frac{M^3}{\pi^{1.5}} \sqrt{A_R t_r A_F t_f} \quad (21)$$

Thus, when the total time is optimised, it is equally divided between the real and reciprocal space parts of the calculation. This is verified in Fig. 3 (b), which displays plots of T_R , T_F and T as a function of N , at $x = 1/6$ and for $N_b = 10$, $c = 4.44c^*$ and $M = 3.3$. Symbols indicate simulation data and solid lines correspond to Eq. (21) with the appropriate values for the various parameters. Eq. (21) also indicates that the real space, reciprocal space and total time scale as $N^{1.5}$. Simulation results shown in Fig. 3 (b) substantiate this prediction. These results are similar to those obtained by Fincham [42] in the context of electrostatic interactions.

IV. DECOMPOSITION OF THE DIFFUSION TENSOR

In component form, the decomposition rule (Eq. (2)) for obtaining the block matrix \mathcal{B} can be expressed as follows,

$$\sum_{\beta=1}^N \sum_{q=1}^3 \mathcal{B}_{\nu\beta}^{rq} \mathcal{B}_{\mu\beta}^{sq} = \mathcal{D}_{\nu\mu}^{rs} \quad (22)$$

where $\{\nu, \beta, \mu = 1, \dots, N\}$, $\{r, q, s = 1, 2, 3\}$, and $\mathcal{D}_{\nu\mu}^{rs}$ is the ' rs 'th Cartesian component of the tensor $\mathcal{D}_{\nu\mu}$. The matrix \mathcal{B} is not unique. Assuming that \mathcal{B} is a lower (or upper) triangular matrix leads to its calculation using a Cholesky decomposition of \mathcal{D} , which as mentioned earlier, requires $O(N^3)$ operations. Fixman's [24] approach achieves an attenuation of this CPU intensity by recognising that (i) it is sufficient to find \mathcal{B} approximately, and (ii) the individual columns of the matrix \mathcal{B} are in themselves not of much interest, only the vector $d\mathcal{S} = \mathcal{B} \cdot \Delta\mathcal{W}$ is required, where $\Delta\mathcal{W}$ is a vector consisting of the $3N$ Gaussian noise coordinates ΔW_μ^s , with $\mu = 1, \dots, N$, and $s = 1, 2, 3$. By assuming that $\mathcal{B} = \sqrt{\mathcal{D}}$, and using a Chebyshev polynomial approximation for the square root function, Fixman showed that [24–26, 53]

$$d\mathcal{S} = \sqrt{\mathcal{D}} \cdot \Delta\mathcal{W} \approx \sum_{p=0}^{N_{\text{Ch}}-1} c_p \mathbf{v}_p - \frac{c_0}{2} \Delta\mathcal{W} \quad (23)$$

where N_{Ch} is the number of terms used in the Chebyshev polynomial approximation, c_p are the Chebyshev coefficients, and the vectors \mathbf{v}_p are defined by the recurrence relations

$$\mathbf{v}_p = 2\mathcal{Y} \cdot \mathbf{v}_{p-1} - \mathbf{v}_{p-2}; \quad p \geq 2 \quad (24)$$

with $\mathbf{V}_0 = \Delta \mathbf{W}$ and $\mathbf{V}_1 = \mathbf{Y} \cdot \mathbf{V}_0$. The linear mapping

$$\mathbf{Y} = \left(\frac{2}{d_{\max} - d_{\min}} \right) \mathbf{D} - \left(\frac{d_{\max} + d_{\min}}{d_{\max} - d_{\min}} \right) \mathcal{I} \quad (25)$$

(where \mathcal{I} denotes the $3N \times 3N$ -dimensional identity matrix), ensures that the eigenvalues of \mathbf{Y} lie in the domain $[-1, 1]$ when the eigenvalues of \mathbf{D} are within $[d_{\min}, d_{\max}]$. This is essential for the validity of the Chebyshev approximation.

It is clear that for a given N_{Ch} , the cost of the direct calculation of the $3N$ -dimensional vector $d\mathbf{S}$, without the intermediate calculation of \mathbf{B} , is proportional to $N_{\text{Ch}} \times$ [the cost of evaluating \mathbf{V}_p]. The number of terms N_{Ch} that are required is determined by the desired accuracy in the estimation of the square root. The choice of N_{Ch} is also affected by the necessity of ensuring that the bounds d_{\max} and d_{\min} satisfy the following constraints relative to the maximum (λ_{\max}) and minimum (λ_{\min}) eigenvalues of \mathbf{D} , namely, $d_{\max} \geq \lambda_{\max}$ and $d_{\min} \leq \lambda_{\min}$.

The CPU cost involved in adopting Fixman's procedure for dilute polymer solutions have been discussed in depth in Refs. 25, 26, and 53. Here, we briefly summarise the main conclusions: (i) The cost of evaluating \mathbf{V}_p is simply $O(N^2)$. (ii) The number of terms in the Chebyshev approximation is determined using the expression [26, 27]

$$N_{\text{Ch}} = \text{nint} \left[\left(\frac{\lambda_{\max}}{\lambda_{\min}} \right)^{\frac{1}{2}} \right] + 1 \quad (26)$$

where nint is the nearest integer function. The use of Eq. (26) is motivated by the finding [24, 25] that the value of N_{Ch} required to keep the error in the estimation of the square root below a fixed tolerance, scales as $(\lambda_{\max}/\lambda_{\min})^{\frac{1}{2}}$. (iii) The limiting eigenvalues λ_{\max} and λ_{\min} can be calculated exactly in $O(N^2)$ operations using standard software packages—this procedure was adopted in Ref. 25 with the package ARPACK. On the other hand, Kröger *et al.* [26] and Prabhakar and Prakash [27] avoid explicit evaluation of the eigenvalues, but instead obtain approximate estimates for λ_{\max} and λ_{\min} . In particular, Prabhakar and Prakash [27] use the following expressions based on a suggestion by Fixman [24]

$$\begin{aligned} \lambda_{\max}^{\text{Fixman}} &= \frac{1}{3N} (\mathbf{U}^+ \cdot \mathbf{D} \cdot \mathbf{U}^+) \quad \text{and} \\ \lambda_{\min}^{\text{Fixman}} &= \frac{1}{3N} (\mathbf{U}^- \cdot \mathbf{D} \cdot \mathbf{U}^-) \end{aligned} \quad (27)$$

where \mathbf{U}^+ is a $3N$ -dimensional vector, all of whose elements are equal to 1 and \mathbf{U}^- is a $3N$ -dimensional vector with alternating 1's and -1 's. Further, the bounds $d_{\max} = 2\lambda_{\max}^{\text{Fixman}}$ and $d_{\min} = 0.5\lambda_{\min}^{\text{Fixman}}$ were chosen to satisfy the conditions on the magnitudes of d_{\max} and d_{\min} relative to the maximum and minimum eigenvalues. Since for dilute polymer solutions, $(\lambda_{\max}/\lambda_{\min}) \sim N^{0.5}$ and consequently $N_{\text{Ch}} \sim N^{1/4}$, the CPU-time requirement for the calculation of $d\mathbf{S}$ in Fixman's method scales as $N_{\text{Ch}}N^2 \sim N^{9/4}$.

In the case of semidilute polymer solutions, since determining \mathbf{V}_p requires the recursive evaluation of the product of a linear transformation of the diffusion tensor with various $3N$ -dimensional vectors (see Eq. (24)), the Ewald sum can be used for its evaluation, with the force vector \mathbf{F}_μ in Eq. (7) replaced by the relevant vector in the Chebyshev recursive relationship Eq. (24). Thus the cost of evaluating \mathbf{V}_p is identical to the cost of carrying out the Ewald sum. With the optimisation introduced here, this would imply a cost that scales as $O(N^{1.5})$. The issues of determining the number of terms N_{Ch} , and the maximum and minimum eigenvalues of \mathbf{D} , must also be addressed before the total cost of Fixman's procedure in the context of semidilute solutions can be estimated.

As pointed out earlier, it is not necessary to know the diffusion matrix \mathbf{D} explicitly in order to describe the conformational evolution of polymer molecules in a semidilute solution. However, since Beenakker [29] provides an expression for the periodic diffusion tensor $\mathbf{D}_{\nu\mu}$ in his original derivation, it can be used to determine the exact values of the maximum and minimum eigenvalues, denoted here by $\lambda_{\max}^{\text{exact}}$ and $\lambda_{\min}^{\text{exact}}$. By comparing the values given by Eqs. (27) with the exact values (obtained with the `gsl_eigen_symm` subroutine of the GNU Scientific Library), we find that the behaviour for our semidilute system is quite different from what is known for single-chain simulations: While in the latter case, $\lambda_{\max}^{\text{Fixman}}$ is a reasonable approximation to $\lambda_{\max}^{\text{exact}}$ (meaning that it scales in the same way with the number of beads, with a constant ratio of order unity), we here find that $\lambda_{\max}^{\text{Fixman}}$ is essentially independent of N , while $\lambda_{\max}^{\text{exact}}$ increases with N , roughly like $N^{0.6}$. In other words, Eq. (27) provides only a poor approximation. The reason why the behaviour is so different for dilute and semidilute systems is not clear to us; we speculate that it might have to do with the different density distributions of segments. Nevertheless, we can still use $\lambda_{\max}^{\text{Fixman}}$ for estimating the maximum eigenvalue, since we empirically find, for a range of values of c/c^* , a , N_b and N_c , and for a variety of polymer conformations, the relation

$$\lambda_{\max}^{\text{exact}} = 0.35 N^{0.6} \lambda_{\max}^{\text{Fixman}} \quad (28)$$

which is therefore used to estimate λ_{\max} , assuming that it is valid throughout. Similarly, we find empirically that the lowest exact eigenvalue is essentially independent of the number of segments, i.e.

$$\frac{\lambda_{\max}^{\text{exact}}}{\lambda_{\min}^{\text{exact}}} = C N^{0.6} \quad (29)$$

where the pre-factor C depends on the values of c/c^* , a and N_b , increasing with an increase in a and N_b and decreasing with an increase in c/c^* . For instance, for $c = 4.44c^*$, $a = 0.5$ and $N_b = 10$, we find $C = 8$. It follows that in the course of simulations a fairly accurate estimate of the minimum eigenvalue can be obtained, once λ_{\max} is determined, by using the expression $\lambda_{\min} = \lambda_{\max}/(C N^{0.6})$. In general, the value of C is

obtained by trial and error. Once λ_{\max} and λ_{\min} are determined by this procedure, we find that it is adequate to use the bounds $d_{\max} = \lambda_{\max}$ and $d_{\min} = \lambda_{\min}$ to ensure a robust implementation of the Chebychev polynomial approximation.

With regard to the number of Chebyshev terms, we find that for semidilute solutions, as in the case of dilute solutions, the value of N_{Ch} required to keep the error in the estimation of the square root below a fixed tolerance, scales as $(\lambda_{\max}/\lambda_{\min})^{\frac{1}{2}}$. This immediately suggests from Eq. (29) that the CPU-time requirement for the calculation of $d\mathcal{S}$ for semidilute solutions using Fixman's method scales as $N_{\text{Ch}}N^{1.5} \sim N^{1.8}$. Equation (26) is used here to provide an initial guess for N_{Ch} , which is then incrementally increased until the relative error E_f in the estimation of the square root function, given by the following expression suggested in Ref. 25,

$$E_f = \left(\frac{|\mathbf{B} \cdot \Delta \mathbf{W} \cdot \mathbf{B} \cdot \Delta \mathbf{W} - \Delta \mathbf{W} \cdot \mathcal{D} \cdot \Delta \mathbf{W}|}{\Delta \mathbf{W} \cdot \mathcal{D} \cdot \Delta \mathbf{W}} \right)^{1/2} \quad (30)$$

is less than a specified tolerance. In practice we find that the choice of C affects the efficiency with which the final value of N_{Ch} is obtained.

V. OPTIMISATION OF EACH EULER TIME STEP

The implementation of the Euler algorithm used here to determine the configurational evolution of the system requires the estimation of the drift term $\sum_{\mu} \mathbf{D}_{\nu\mu} \cdot \mathbf{F}_{\mu}$ and the diffusion term $\sum_{\mu} \mathbf{B}_{\nu\mu} \cdot \Delta \mathbf{W}_{\mu}$ at each time step, since the algorithm proceeds by evaluating the right hand side of Eq. (1) for each bead ν in the original simulation box. As mentioned earlier, determining the latter sum involves the repeated invocation of the Ewald sum. Since the spatial configuration of the system is frozen in a single time step, all terms in the Ewald sum that are either (i) constant, (ii) only dependent on the reciprocal space vector \mathbf{k} , or (iii) only dependent on the spatial configuration, do not have to be repeatedly evaluated. As a result, it becomes necessary not only to discuss the optimal evaluation and scaling with system size of the drift and diffusion terms individually (as we have in Secs. III and IV), but also to consider the overall optimisation of each Euler time step.

It turns out that there are two ways in which this optimisation can be carried out. In order to give a flavour of the issues involved, we only discuss here the treatment of the term involving $\mathbf{M}^{(1)}(\mathbf{r}_{\nu\mu,\mathbf{n}})$ in the Ewald sum (see Eq. (14)). The remaining terms are either treated similarly, or entail a more straightforward treatment. Clearly, the term involving $\mathbf{M}^{(1)}(\mathbf{r}_{\nu\mu,\mathbf{n}})$ is first evaluated when the drift term $\sum_{\mu} \mathbf{D}_{\nu\mu} \cdot \mathbf{F}_{\mu}$ is evaluated. Subsequently, it is required each time the term $\mathcal{D} \cdot \mathcal{V}_p$; $p = 0, \dots, N_{\text{Ch}} - 1$ is evaluated in the Chebychev polynomial approximation (see Eqs. (24) and (25)). For ease of discussion, we denote

by \mathcal{V}_{μ}^s the $3N$ components of a typical vector \mathcal{V}_p . Then the term involving $\mathbf{M}^{(1)}(\mathbf{r}_{\nu\mu,\mathbf{n}})$ in the implementation of the Chebychev polynomial approximation can be written as $\sum_{\mathbf{n}} \sum_{\mu=1}^N \sum_{s=1}^3 M_{\nu\mu,\mathbf{n}}^{rs} \mathcal{V}_{\mu}^s$, where $M_{\nu\mu,\mathbf{n}}^{rs}$ represents the ' rs 'th Cartesian component of the tensor $\mathbf{M}^{(1)}(\mathbf{r}_{\nu\mu,\mathbf{n}})$. Before discussing the two methods of optimisation used here, it is worth noting the following point that is common to both methods. For each bead ν , in any periodic image \mathbf{n} , the sum over the index μ is carried out only over the nearest neighbours of bead ν , i.e., over the N_{r_c} particles that lie within a sphere centred at bead ν with cutoff radius r_c . The choice of r_c , however, is different in the two schemes, as detailed below.

In the first method of optimisation, which we denote here as HMA (for "High Memory Algorithm"), the $3N \times 3N$ matrix $S_{\nu\mu}^{rs} = \sum_{\mathbf{n}} M_{\nu\mu,\mathbf{n}}^{rs}$ is calculated once and for all and stored in the course of evaluating the drift term $\sum_{\mu} \mathbf{D}_{\nu\mu} \cdot \mathbf{F}_{\mu}$. Note that the cost of evaluating $S_{\nu\mu}^{rs}$ scales as $O(N \times N_{r_c})$ since in each periodic image \mathbf{n} , only the beads μ whose distance from bead ν is less than a cutoff radius $(r_c^{\text{HMA}})_{\text{opt}}$ are considered in the sum over all periodic images. The nature of $(r_c^{\text{HMA}})_{\text{opt}}$ and the value of N_{r_c} in this context, is discussed in more detail below. It should be noted that the matrix $S_{\nu\mu}^{rs}$ becomes increasingly sparse when the system size is increased. While it is therefore possible to save memory by sparse-matrix techniques (meaning in practice the construction of a Verlet table [52] and making use of indirect addressing), this was not attempted here, i.e. we stored the matrix with a simple $O(N^2)$ implementation. Subsequently, each time the term $\mathcal{D} \cdot \mathcal{V}_p$; $p = 0, \dots, N_{\text{Ch}} - 1$ is calculated in the Chebychev polynomial approximation, the $O(N^2)$ matrix multiplication $\sum_{\mu=1}^N \sum_{s=1}^3 S_{\nu\mu}^{rs} \mathcal{V}_{\mu}^s$ is carried out. Again, a sparse matrix implementation might be able to reduce this computational complexity. Ultimately this term dominates and the total CPU cost of this scheme scales as $O(N_{\text{Ch}} \times N^2)$. For systems that are not sufficiently large, the CPU cost might lie in the crossover region between $O(N \times N_{r_c})$ (the cost for the deterministic drift) and $O(N_{\text{Ch}} \times N^2)$.

The reason that $(r_c^{\text{HMA}})_{\text{opt}}$ is different from the cutoff radius $(r_c^{\text{E}})_{\text{opt}}$ (calculated earlier for just the evaluation of the Ewald sum) is because in the HMA algorithm a different procedure is used in the repeated evaluation of the Ewald sum, with certain quantities being calculated once and for all and stored. By repeating the procedure adopted earlier for optimising the bare Ewald sum, namely, by estimating the total time required to evaluate the various quantities in the real space and reciprocal space sums, we find for the CPU time for one step in nanoseconds

$$T^{\text{HMA}}/ns = 30N(N-1) + 1500N r_c^3 c + 23N^2(2 + N_{\text{Ch}}) + 0.67 \frac{M^6}{r_c^3 c} N^2 (9.2 + 4.2N_{\text{Ch}}) \quad (31)$$

where the constants reflect the various execution times

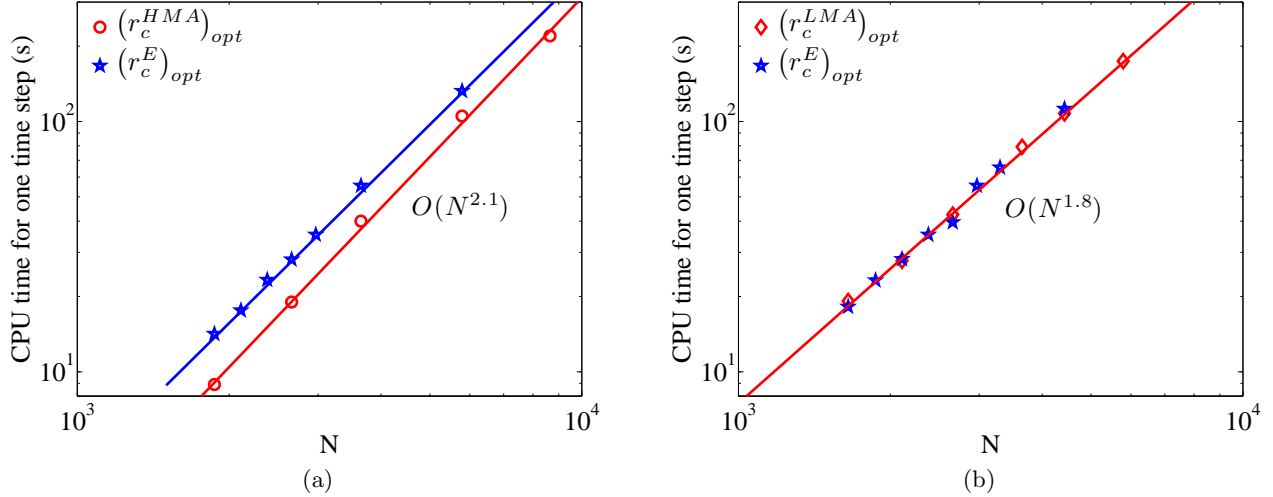


FIG. 4. (Color online) CPU time scalings for (a) HMA (b) LMA. Symbols represent simulations results, and the lines are analytical estimates for the total time.

for individual terms on a 156 SGI Altix XE 320 cluster. Minimising this with respect to the cutoff radius leads to

$$(r_c^{\text{HMA}})_{\text{opt}}^3 c = \frac{M^3}{8} [0.25N + 0.12NN_{\text{Ch}}]^{1/2} \quad (32)$$

It turns out that $(r_c^{\text{HMA}})_{\text{opt}} > (r_c^{\text{E}})_{\text{opt}}$. This is because a major part of the real space calculation of $\sum_{\mathbf{n}} \mathbf{M}^{(1)}(\mathbf{r}_{\nu\mu,\mathbf{n}})$ and $\mathbf{M}^*(\mathbf{r}_{\nu\mu,\mathbf{n}} = \mathbf{o})$ is not repeated N_{Ch} times in the HMA, leading to a cheaper real space implementation. As a result, the optimisation procedure allows the HMA to attribute a greater computational load to the real space sum relative to the reciprocal space sum by having a larger cutoff radius than $(r_c^{\text{E}})_{\text{opt}}$. In contrast to the bare Ewald sum, where $N_{r_c} \sim N^{0.5}$, we find empirically that in the HMA, $N_{r_c} \sim N^{0.7}$.

It is clear from Fig. 4 (a) that the CPU time for HMA scales as $O(N^{2.1})$ when the simulation is run at a cutoff radius of $(r_c^{\text{HMA}})_{\text{opt}}$, with the empirically estimated exponent 2.1 lying in the crossover regime discussed earlier. Figure 4 (a) also indicates that the CPU cost is greater when $(r_c^{\text{E}})_{\text{opt}}$ is used in the HMA, confirming the necessity to optimise the total procedure for evaluating a single Euler time step rather than using the cutoff radius obtained from the Ewald sum optimisation.

The major difference from the HMA, in the alternative method of optimisation used here (denoted by LMA for “Low Memory Algorithm”), is the treatment of the sum $\sum_{\mathbf{n}} \sum_{\mu=1}^N \sum_{s=1}^3 M_{\nu\mu,\mathbf{n}}^{rs} \mathcal{V}_{\mu}^s$. While many quantities, such as those that are constant, or only functions of the reciprocal space vector \mathbf{k} , are still calculated and stored once and for all when the drift term $\sum_{\mu} \mathbf{D}_{\nu\mu} \cdot \mathbf{F}_{\mu}$ is evaluated, the $3N \times 3N$ matrix $S_{\nu\mu}^{rs}$ is not stored. Instead, the following two steps are carried out: (i) For a given bead index ν and periodic image \mathbf{n} , the quantity $T_{\nu,\mathbf{n}}^r = \sum_{\mu=1}^N \sum_{s=1}^3 M_{\nu\mu,\mathbf{n}}^{rs} \mathcal{V}_{\mu}^s$ is evaluated, ensuring

that only those beads μ that lie within a cutoff radius $(r_c^{\text{LMA}})_{\text{opt}}$ of bead ν are considered in the sum over μ . Note that for each bead μ , the sum over s involves a simple $(3 \times 3) \times (3 \times 1)$ matrix multiplication. (ii) The sum $\sum_{\mathbf{n}} T_{\nu,\mathbf{n}}^r$ over periodic images \mathbf{n} is then performed to obtain the required quantity in the Ewald sum.

Since, even in the LMA, some quantities are stored during the evaluation of the drift term $\sum_{\mu} \mathbf{D}_{\nu\mu} \cdot \mathbf{F}_{\mu}$, we can optimise the entire process involved in executing one time step in the Euler algorithm by choosing the appropriate cutoff radius. Adopting the procedure described earlier, we find for the CPU time per step in nanoseconds

$$T^{\text{LMA}}/ns = 1200 r_c^3 c N(1 + N_{\text{Ch}}) + 2 \frac{M^6}{r_c^3 c} N^2 (1.8 + 1.5N_{\text{Ch}}) \quad (33)$$

$$(r_c^{\text{LMA}})_{\text{opt}}^3 c = \frac{M^3}{8} \left[\frac{0.18N + 0.15NN_{\text{Ch}}}{1 + N_{\text{Ch}}} \right]^{1/2} \quad (34)$$

Figure 4 (b) compares the CPU cost involved when either the cutoff radius $(r_c^{\text{LMA}})_{\text{opt}}$ or $(r_c^{\text{E}})_{\text{opt}}$ is used in the LMA. The reason that $(r_c^{\text{LMA}})_{\text{opt}}$ and $(r_c^{\text{E}})_{\text{opt}}$ are nearly equal to each other is because practically all the time consuming parts of the Ewald sum are calculated repeatedly N_{Ch} times in the LMA. As a result, in contrast to the HMA, the saving achieved by storing some quantities does not make a significant difference to the choice of cutoff radius.

Unlike the HMA, there is no large storage requirement in the LMA, as shown in Fig. 5 (a), where it is seen to scale as $O(N)$ for sufficiently large N . Further, the CPU cost scales as $O(N_{\text{Ch}} \times N \times N_{r_c})$, which is identical to the scaling for the basic Ewald sum, namely, $O(N^{1.8})$ as can be seen in Fig. 5 (b). On the other hand, since $S_{\nu\mu}^{rs}$

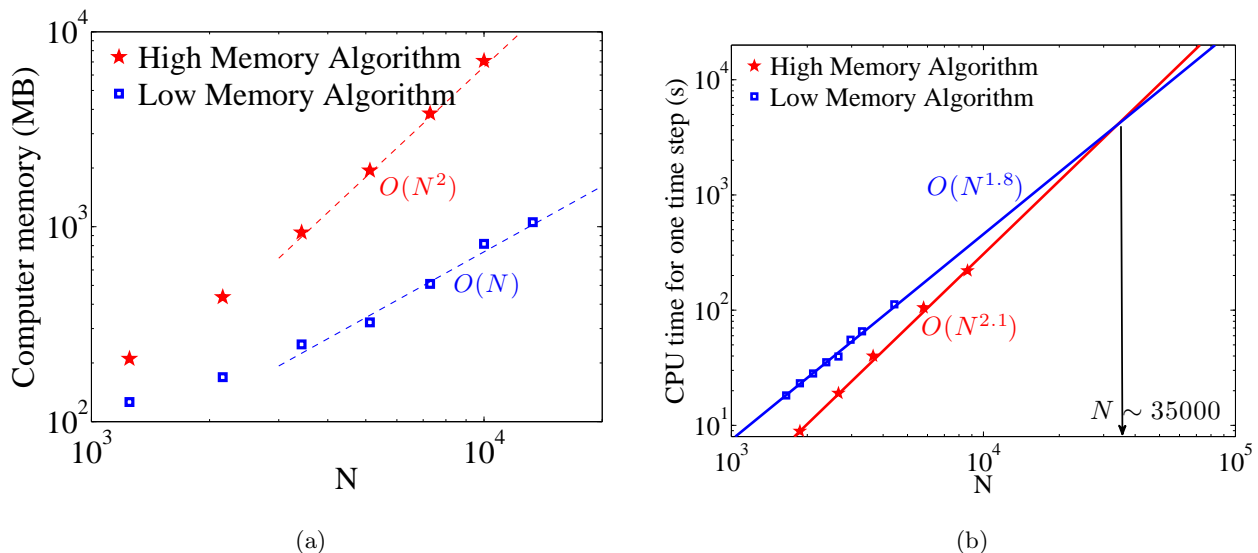


FIG. 5. (Color online) Comparison between HMA and LMA for (a) Computer memory requirement (b) CPU time required for a single time step computation

is not stored, the components $M_{\nu\mu,\mathbf{n}}^{rs}$ are repeatedly evaluated in each of the recursive Chebychev calculations. This extra calculation leads to a large pre-factor in the scaling of the CPU with N . However, at $N \sim 35000$ a crossover in the CPU cost can be seen to occur, suggesting that it is advisable to use HMA below a system size of roughly 35000, while the LMA would be cheaper for larger systems.

VI. TESTING AND VERIFICATION

The optimised BD algorithm developed here is validated by testing and verification under both θ -solvent and good solvent conditions. In the former case, we first check to see if static equilibrium properties, namely, the radius of gyration and the end-to-end vector, agree with known analytical results. Secondly, the current implementation of the Ewald sum for hydrodynamic interactions (which enables its use even in simulations that do not incorporate excluded-volume interactions) is tested by comparing the prediction of the infinite dilution equilibrium self-diffusion coefficient, which is a dynamic property, with the results of a BD simulation of single chain dynamics. As mentioned in Sec. I, we have recently quantitatively compared the predictions of the explicit solvent LB/MD method with the predictions of the implicit solvent BD method for the dynamics of a single chain under good solvent conditions in the dilute limit [21]. A natural follow up of the development of the current BD algorithm is to compare the two methods at finite concentrations under good solvent conditions. Here we extend our earlier study by comparing the predictions of the radius of gyration, the end-to-end vector, and the self-diffusion coefficient. This serves both to verify the predictions of

the current algorithm in a regime where there are no analytical predictions, and to obtain an estimate of the relative computational costs of the two mesoscopic simulation methods in the semidilute regime.

The mean-square end-to-end distance is given by

$$\langle R_e^2 \rangle = \langle (\mathbf{r}_{N_b} - \mathbf{r}_1)^2 \rangle \quad (35)$$

while the mean-square radius of gyration is given by

$$\langle R_g^2 \rangle = \frac{1}{2N_b^2} \sum_{\mu=1}^{N_b} \sum_{\nu=1}^{N_b} \langle r_{\mu\nu}^2 \rangle \quad (36)$$

with $r_{\mu\nu} = |\mathbf{r}_\nu - \mathbf{r}_\mu|$ being the inter-particle distance. The long-time self-diffusion coefficient is calculated by tracking the mean-square displacement of the centre of mass \mathbf{r}_c of each chain

$$D_L = \lim_{t \rightarrow \infty} \left\langle \frac{|\mathbf{r}_c(t) - \mathbf{r}_c(0)|^2}{6t} \right\rangle \quad (37)$$

The predictions of the radius of gyration, the end-to-end vector, and the self-diffusion coefficient by the current algorithm under θ -solvent and good solvent conditions, and their verification by various means, are discussed in turn below.

A. θ -solvents

The mean-square end-to-end distance and the mean-square radius of gyration at equilibrium were obtained by carrying out simulations of bead-spring chains with Hookean springs, using $N_b = 20$ and 40 and a fixed number of chains $N_c = 20$. The non-dimensional bead-radius

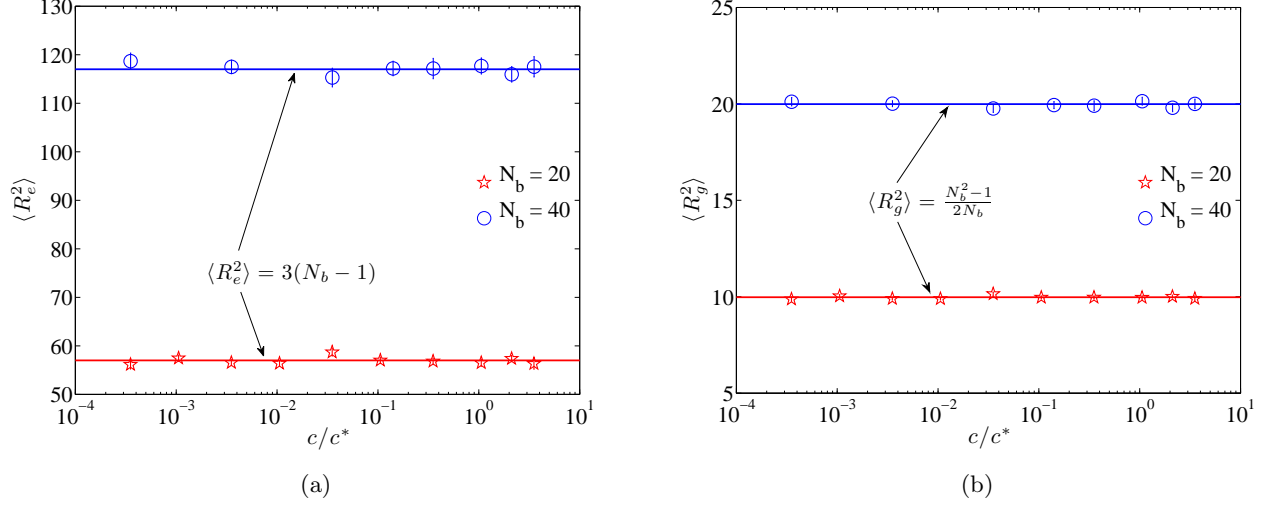


FIG. 6. (Color online) Validation of static properties under θ -conditions: (a) Mean-square end-to-end distance $\langle R_e^2 \rangle$ (b) Mean-square radius of gyration $\langle R_g^2 \rangle$. Symbols indicate simulation data, while solid lines represent the analytical results given by Eqs. (38) and (39).

a was chosen to be 0.5, and a time step $\Delta t = 0.01$ was used to carry out the Euler integration. A range of concentrations from $3 \times 10^{-4} c^*$ to $3 c^*$ were considered, with the concentration being varied by changing the size of the simulation box L . Since the chains are free to cross each other for θ -solvents, static properties such as the end-to-end distance and the radius of gyration are independent of concentration. Further, as is well known, their dependence on N_b can be shown analytically to be [49]

$$\langle R_e^2 \rangle = 3(N_b - 1) \quad (38)$$

and

$$\langle R_g^2 \rangle = \frac{N_b^2 - 1}{2N_b} \quad (39)$$

Note that c^* can be determined once a choice for N_b is made.

Figures 6 (a) and (b) display the results for $\langle R_e^2 \rangle$ and $\langle R_g^2 \rangle$, respectively, for the range of concentrations considered here. Symbols indicate simulation data, while solid lines represent the analytical results given by Eqs. (38) and (39). Clearly, the simulated static properties are in good agreement with analytical predictions.

The single chain diffusion coefficient in a dilute solution under θ -solvent conditions is used here as the benchmark for verifying the current implementation of the Ewald sum. The value of the diffusion coefficient for $N_b = 20$ and $a = 0.5$ is displayed as the solid line in Fig. 7, obtained here by a conventional BD simulation algorithm that uses a semi-implicit predictor corrector scheme developed in our group for simulating a single chain that is not confined in a box [27]. For the same set of input simulation parameters, the long-time diffusivity is obtained from the current multi-particle BD algorithm for a range

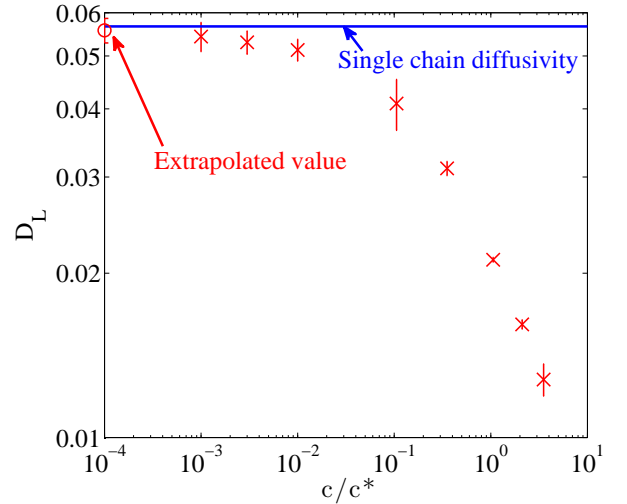


FIG. 7. (Color online) Long-time self-diffusion coefficient under θ -solvent conditions. Symbols indicate simulation data obtained with the current multi-particle algorithm, while the solid line represents the value obtained by simulating the dynamics of a single chain in a dilute solution. The circle symbol on the y -axis is the value obtained by extrapolating the finite concentration results to the limit of zero concentration.

of concentrations. It is clear from Fig. 7 that the simulated data (symbols) for the diffusivity D_L approaches the single chain result in the limit of zero concentration. The value of D_L at $c/c^* = 0$ was obtained by fitting the values at $c/c^* = 0.001, 0.003$ and 0.01 with a second order polynomial and extrapolating to zero concentration.

TABLE I. Comparison of predictions of the radius of gyration, the end-to-end vector, and the self-diffusion coefficient by the explicit solvent LB/MD method with the predictions of the implicit solvent BD method, for a bead-spring chain with $N_b = 10$ at three different concentrations, in a good solvent. Note that all properties are given in BD units, except the box size L , and concentration c , which are given in LB units when reported for the LB/MD simulations. Both L and c are identical in both methods when reported in the same unit system. Note that the highest concentration corresponds to melt-like conditions.

N_c	Method	L	c	c/c^*	$\langle R_e^2 \rangle$	$\langle R_g^2 \rangle$	D_L
20	BD	24.152	0.0142	0.546 ± 0.001	111.37 ± 0.47	18.36 ± 0.04	$0.0272 \pm 6 \times 10^{-4}$
	LB	10	0.2	0.543 ± 0.005	112.93 ± 0.27	18.29 ± 0.02	$0.0268 \pm 8 \times 10^{-4}$
32	BD	21.737	0.0311	1.199 ± 0.002	98.35 ± 0.43	16.6 ± 0.04	$0.0162 \pm 6 \times 10^{-4}$
	LB	9	0.439	1.192 ± 0.011	99.11 ± 0.36	16.59 ± 0.03	$0.0151 \pm 4 \times 10^{-4}$
70	BD	21.737	0.068	2.623 ± 0.004	76.07 ± 0.53	13.33 ± 0.05	$0.0024 \pm 1 \times 10^{-4}$
	LB	9	0.96	2.607 ± 0.025	77.29 ± 0.35	13.42 ± 0.04	$0.00245 \pm 5 \times 10^{-5}$

B. Good solvents

In order to carry out a quantitative comparison between the LB/MD and BD methods, it is necessary to ensure that the underlying polymer model is identical for both the methods, and to map the input parameters of the hybrid model onto the input values of the BD model. A detailed discussion of how this can be achieved in the context of dilute solutions has been given in Ref. 21. Exactly the same procedure has been adopted here. Essentially, a bead-spring chain with FENE springs is used, with a Weeks-Chandler-Andersen potential, which acts between all monomers, employed to model the excluded-volume (EV) effect. While in the LB/MD simulation approach, the Weeks-Chandler-Andersen parameters are used to define the units of energy, length, and time, the corresponding units in the BD simulations have been discussed earlier in Sec. II A. We refer readers to Ref. 21 for details of the length and time unit conversions between the two methods. The comparison of the two methods proceeds by first picking the simulation parameters for the LB/MD model, using these for the LB/MD simulations, then converting them to BD units using the procedure outlined in Ref. 21, and finally running the equivalent BD model obtained in this manner. In other words, the two units systems are maintained in the respective methods, and a comparison of predicted quantities carried out *a posteriori*.

The results of carrying out this procedure for $\langle R_e^2 \rangle$, $\langle R_g^2 \rangle$ and D_L are shown in Table (I) for $N_b = 10$ at three different concentrations. It is worth noting that, since EV interactions are short-ranged, we have implemented a neighbour-list in the current BD algorithm for computing the pairwise summation of EV interactions, with a cutoff radius equal to the range of the Weeks-Chandler-Andersen potential. All values are reported in BD units, unless specified otherwise. We find it convenient to maintain the same absolute concentration in the two methods rather than the same c/c^* , as this would entail an interpolation procedure. In the BD method, c^*

is determined from $\langle R_g^2 \rangle$ in the dilute limit, by carrying out a single chain simulation for parameter values that are identical to those in the multi-particle BD simulation. In the LB/MD method, simulations are carried out for three box sizes, $L = 12, 17$ and 21 , with the number of monomers held fixed (we use $N_c = 20$ and $N_b = 10$). As a result, the monomer concentration decreases with increasing box size. The values of $\langle R_g^2 \rangle$ obtained for these three box sizes are extrapolated to infinite box size in order to determine $\langle R_g^2 \rangle$ (and consequently c^*) in the dilute limit.

It is clear from Table (I), both in the dilute limit, with regard to values of c/c^* , and at all three finite concentrations, with regard to values of $\langle R_e^2 \rangle$, $\langle R_g^2 \rangle$ and D_L , that there is excellent agreement between the two mesoscopic simulation methods, since all properties agree with each other within error bars. This validates the current algorithm in a regime where there are no analytical solutions. Further, it demonstrates the robustness of the parameter mapping technique developed by Pham *et al.* [21] for comparing the two simulation methods.

VII. COMPARISON OF COMPUTATIONAL COST WITH LB/MD

Our recent comparison [21] of the predictions of the explicit solvent LB/MD method with the predictions of the implicit solvent BD method for the dynamics of a single chain indicated that in the dilute limit, BD is the method of choice as it is significantly more efficient than LB/MD. However, Fig. 8 suggests that for our current implementation the situation is quite the reverse at the finite concentration, $c/c^* = 1.2$, at which the simulation data in the figure were obtained. The comparison of the two mesoscopic simulation methods displayed in Fig. 8 was carried out using the identical procedure developed earlier by Pham *et al.* [21]. Essentially, the LB/MD method was run for a total of 100 MD time steps (with a step size of 0.01 in LB units, or 0.018 in BD units). This

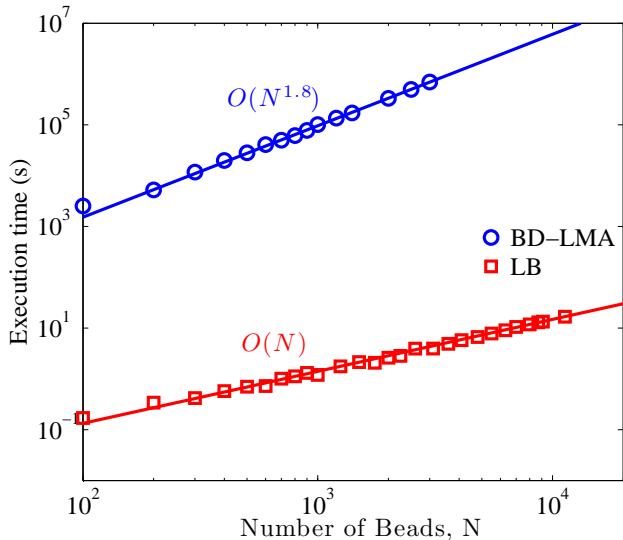


FIG. 8. (Color online) Comparison of the CPU time required by the LB and BD systems for a wide range of system sizes N , at concentration $c/c^* = 1.2$, for the equivalent of one LB time unit.

amounts to a total simulation time of one time unit in terms of LB units. The BD algorithm was then run for the same length of physical time, by converting one LB time unit to BD time units. The BD algorithm required a significantly smaller time step of 10^{-4} in BD units. The reason for this choice is because the current implementation uses a simple Euler integration scheme, with a rejection algorithm that ensures that none of the springs in any of the bead-spring chains exceeds the upper limit of the FENE spring length \sqrt{b} . In contrast, the earlier comparison of the two methods in the dilute limit was based on a BD code that uses a semi-implicit predictor-corrector method, enabling the use of a much larger step size of 50×10^{-4} BD units. The dependence of CPU time on system size was examined here by increasing the number of chains N_c , while keeping the number of beads in a chain fixed at $N_b = 10$. The concentration was maintained constant at $c/c^* = 1.2$ (or $c = 0.031$ in BD units) by increasing the box size L suitably. Since the difference between the HMA and LMA BD algorithms is insignificant on the scale of the difference between LB/MD and BD, only results for the LMA are shown in Fig. 8.

The CPU time scaling of the LMA algorithm has been established in Sec. V to be $N^{1.8}$. From Eqs. (33) and (34) one immediately sees that after optimisation the CPU time depends only on the particle number N , but is independent of the concentration c (or the system volume V):

$$T^{\text{LMA}}(N, V) = \gamma^{\text{LMA}} N^{1.8} \quad (40)$$

with some proportionality constant γ^{LMA} . Conversely, the LB/MD method is dominated by the CPU effort of

the solvent, i.e.

$$T^{\text{LB}}(N, V) = \gamma^{\text{LB}} V = \gamma^{\text{LB}} \frac{N}{c} \quad (41)$$

with another constant γ^{LB} . Hence

$$\frac{T^{\text{LMA}}}{T^{\text{LB}}} = \frac{\gamma^{\text{LMA}}}{\gamma^{\text{LB}}} c N^{0.8} \quad (42)$$

From our CPU timings we find a value $\gamma^{\text{LMA}}/\gamma^{\text{LB}} = 1.3 \times 10^4$ in BD units, i.e. our current implementation of Ewald BD becomes competitive with LB/MD only if the concentration is below the very small value $7.8 \times 10^{-5} \times N^{-0.8}$.

However, it should be noted that the present version is by far not the fastest conceivable BD code. Firstly, we expect that by implementing an implicit integrator the time step may be increased by nearly two orders of magnitude. Secondly, the evaluation of the real-space HI should be substantially faster (both in the LMA and HMA versions) by making use of Verlet tables. Thirdly, the HMA algorithm could then take advantage of sparse-matrix techniques (see also the discussion in Sec. V). Finally, the evaluation of the Fourier part can be speeded up by making use of Fast Fourier Transformation, which, as shown previously, gives rise to a complexity of the total algorithm of $O(N^{1.3} \log N)$ [38, 39]. All together, achieving accelerations by up to three orders of magnitude does not seem unrealistic.

VIII. SUMMARY

A range of issues related to the development of an optimised BD algorithm for simulating the dynamics of semidilute solutions in unbounded domains has been considered here. In particular:

1. It is possible to develop an optimised Ewald method for hydrodynamic interactions that splits the cost of evaluating the real space and reciprocal space sums evenly, leading to a CPU cost that scales as $N^{1.5}$, rather than the N^2 scaling that would result from a straightforward implementation.
2. While Beenakker's original implementation of the Ewald sum is only valid for systems without bead overlap, it can be modified to account for bead overlap, such that θ -solutions can be simulated by switching off excluded-volume interactions. To the best of our knowledge, this is the first implementation of an Ewald sum for the regularised branch of the RPY tensor.
3. As in the case of dilute solutions, the number of Chebychev terms required to maintain a desired accuracy scales as $(\lambda_{\max}/\lambda_{\min})^{\frac{1}{2}}$, where λ_{\max} and λ_{\min} are the maximum and minimum eigenvalues of the diffusion tensor \mathcal{D} . It is shown that this leads

to an additional computational load that scales as $N^{0.3}$.

4. It is necessary to consider the optimisation of the overall time required to perform one Euler time step, in addition to the individual optimisations of the Ewald sum and Chebychev polynomial approximation. In this context, two different schemes for optimisation have been proposed in the form of the “high memory” (HMA), and the “low memory” (LMA) algorithms. While the LMA leads to an overall CPU time scaling of $N^{1.8}$, which appears better than the $N^{2.1}$ scaling of the HMA, the large prefactor in the former makes it preferable only for large systems with more than roughly 35,000 particles.
5. The optimised BD algorithm gives accurate predictions under both θ and good solvent conditions. In the latter case, BD predictions are compared with those of the LB/MD method. The parameter mapping scheme developed by Pham *et al.* [21] for dilute solutions is found to be valid and useful even at a

finite concentration in the semidilute regime.

6. In contrast to dilute solutions, where BD was shown to be significantly more computationally efficient than LB/MD [21], exactly the opposite is true for semidilute solutions. The CPU cost of the BD method scales as $N^{1.8}$, while the cost of the LB/MD method scales linearly with system size. The necessity of carrying out an Ewald sum renders the BD method developed here significantly more computationally expensive than LB/MD. Nevertheless, it should be noted that the BD method can be further refined and dramatically speeded up, as discussed at the end of Sec. VII.

ACKNOWLEDGMENTS

The authors gratefully acknowledge CPU time grants from the National Computational Infrastructure (NCI) facility hosted by Australian National University, and Victorian Life Sciences Computation Initiative (VLSCI) hosted by University of Melbourne. The authors would also like to thank John Brady for very helpful discussions.

-
- [1] P. G. De Gennes, *Macromolecules* **9**, 587 (1976).
 - [2] P. G. De Gennes, *Macromolecules* **9**, 594 (1976).
 - [3] P. G. de Gennes, *Scaling Concepts in Polymer Physics* (Cornell University, Ithaca, New York, 1979).
 - [4] M. Muthukumar and S. Edwards, *Polymer* **23**, 345 (1982).
 - [5] M. Muthukumar and S. F. Edwards, *J. Chem. Phys.* **76**, 2720 (1982).
 - [6] M. Muthukumar and S. F. Edwards, *Macromolecules* **16**, 1475 (1983).
 - [7] S. F. Edwards and M. Muthukumar, *Macromolecules* **17**, 586 (1984).
 - [8] M. Rubinstein and R. H. Colby, *Polymer Physics* (Oxford University Press, 2003).
 - [9] P. Ahlrichs, R. Everaers, and B. Dünweg, *Phys. Rev. E* **64**, 040501 (2001).
 - [10] C. Stoltz, J. J. de Pablo, and M. D. Graham, *J. Rheol.* **50**, 137 (2006).
 - [11] C.-C. Huang, R. G. Winkler, G. Sutmann, and G. Gompper, *Macromolecules* **43**, 10107 (2010).
 - [12] J. G. Kirkwood and J. Riseman, *J. Chem. Phys.* **16**, 565 (1948).
 - [13] K. F. Freed and S. F. Edwards, *J. Chem. Phys.* **61**, 3626 (1974).
 - [14] M. Bixon, *Annu. Rev. Phys. Chem.* **27**, 65 (1976).
 - [15] P. Ahlrichs and B. Dünweg, *J. Chem. Phys.* **111**, 8225 (1999).
 - [16] B. Dünweg and A. J. C. Ladd, *Adv. Polym. Sci.* **221**, 89 (2009).
 - [17] A. Malevanets and R. Kapral, *J. Chem. Phys.* **110**, 8605 (1999).
 - [18] R. Kapral, “Multiparticle collision dynamics: Simulation of complex systems on mesoscales,” in *Advances in Chemical Physics* (2008) pp. 89–146.
 - [19] G. Gompper, T. Ihle, D. Kroll, and R. Winkler, *Adv. Polym. Sci.* **221**, 1 (2009).
 - [20] H. C. Öttinger, *Stochastic Processes in Polymeric Fluids* (Springer, Berlin, 1996).
 - [21] T. T. Pham, U. D. Schiller, J. R. Prakash, and B. Dünweg, *J. Chem. Phys.* **131**, 164114 (2009).
 - [22] A. J. C. Ladd, R. Kekre, and J. E. Butler, *Phys. Rev. E* **80**, 036704 (2009).
 - [23] M. Doi and S. F. Edwards, *The Theory of Polymer Dynamics* (Clarendon Press, Oxford, New York, 1986).
 - [24] M. Fixman, *Macromolecules* **19**, 1204 (1986).
 - [25] R. M. Jendrejack, M. D. Graham, and J. J. de Pablo, *J. Chem. Phys.* **113**, 2894 (2000).
 - [26] M. Kröger, A. Alba-Perez, M. Laso, and H. C. Öttinger, *J. Chem. Phys.* **113**, 4767 (2000).
 - [27] R. Prabhakar and J. Prakash, *J. Non-Newtonian Fluid Mech.* **116**, 163 (2004).
 - [28] H. Hasimoto, *J. Fluid Mech.* **5**, 317 (1959).
 - [29] C. W. J. Beenakker, *J. Chem. Phys.* **85**, 1581 (1986).
 - [30] P. P. Ewald, *Annalen der Physik* **369**, 253 (1921).
 - [31] M. Allen and D. Tildesley, *Computer Simulations of Liquids* (Oxford Science, London, 1990).
 - [32] B. A. Luty, M. E. Davis, I. G. Tironi, and W. F. Van Gunsteren, *Mol. Simul.* **14**, 11 (1994).
 - [33] A. Y. Toukmaji and J. A. Board Jr., *Comput. Phys. Commun.* **95**, 73 (1996).
 - [34] M. Deserno and C. Holm, *J. Chem. Phys.* **109**, 7678 (1998).
 - [35] E. Smith, I. Snook, and W. V. Meegen, *Phys. A: Stat. Mech. Appl.* **143**, 441 (1987).
 - [36] J. F. Brady, R. J. Phillips, J. C. Lester, and G. Bossis, *J. Fluid Mech.* **195**, 257 (1988).

- [37] B. Rinn, K. Zahn, P. Maass, and G. Maret, *Europhys. Lett.* **46**, 537 (1999).
- [38] A. Sierou and J. F. Brady, *J. Fluid Mech.* **448**, 115 (2001).
- [39] A. J. Banchio and J. F. Brady, *J. Chem. Phys.* **118**, 10323 (2003).
- [40] J. P. Hernández-Ortiz, J. J. de Pablo, and M. D. Graham, *Phys. Rev. Lett.* **98**, 140602 (2007).
- [41] J. W. Perram, H. G. Petersen, and S. W. De Leeuw, *Mol. Phys.* **65**, 875 (1988).
- [42] D. Fincham, *Mol. Simul.* **13**, 1 (1994).
- [43] J. Rotne and S. Prager, *J. Chem. Phys.* **50**, 4831 (1969).
- [44] H. Yamakawa, *J. Chem. Phys.* **53**, 436 (1970).
- [45] P. Mazur and W. van Saarloos, *Physica A* **115**, 21 (1982).
- [46] P. Sunthar and J. R. Prakash, *Macromolecules* **38**, 617 (2005).
- [47] W. Zylka and H. C. Ottinger, *J. Chem. Phys.* **90**, 474 (1989).
- [48] G. B. Thurston and A. Peterlin, *J. Chem. Phys.* **46**, 4881 (1967).
- [49] R. B. Bird, C. F. Curtiss, R. C. Armstrong, and O. Hassager, *Dynamics of Polymeric Liquids*, Vol. 2 (John Wiley and Sons, New York, 1987).
- [50] R. Hockney, S. Goel, and J. Eastwood, *Chem. Phys. Lett.* **21**, 589 (1973).
- [51] M. Griebel, S. Knapek, and G. Zumbusch, *Numerical Simulation in Molecular Dynamics* (Springer, Berlin, Heidelberg, 2007).
- [52] G. S. Grest, B. Dünweg, and K. Kremer, *Comp. Phys. Comm.* **55**, 269 (1989).
- [53] R. Prabhakar, *Predicting the rheological properties of dilute polymer solutions using bead-spring models: Brownian dynamics simulations and closure approximations*, Ph.D. thesis, Monash University (2005).